PHILOSOPHICAL TRANSACTIONS OF THE ROYAL SOCIETY A MATHEMATICAL, PHYSICAL & ENGINEERING SCIENCES

# Texture and large–strain deformation microstructure

J. Gil Sevillano, C. García Rosales and J. Flaquer Fuster

*Phil. Trans. R. Soc. Lond. A* 1999 **357**, 1603-1619
doi: 10.1098/rsta.1999.0392

THE ROYAL SOCIETY

# Texture and large-strain deformation microstructure

By J. Gil Sevillano, C. García-Rosales and J. Flaquer Fuster

*Centro de Estudios e Investigaciones Técnicas de Guipúzcoa (CEIT) and Faculty of Engineering, University of Navarra, Apdo. 1555, 20009 San Sebastián, Spain* (jgil@ceit.es)

Large-strain plastic deformation at low homologous temperature implies, among other things, severe work hardening, strong crystallographic texturing, microstructural refining, and some degree of macroscopic redundant strain. In most cases, the development of texture does not seem to particularly increase grain interactions above their initial level, which is at the origin of the Hall–Petch effect. Continued strain then leads asymptotically towards an absolute maximum of the tensile flow stress below $G/50$, where $G$ represents the elastic shear modulus.

However, it is well known that some simple deformation textures promote an extraordinary enhancement of the plastic grain interactions that need to be accommodated by monotonically increasing mesoscopic (grain-size range) strain gradients. Such behaviour is accompanied by a concomitant high work-hardening rate and by a remarkable extension of the strengthening limit. The [110] body-centred-cubic or [0001] hexagonal close-packed wire drawing textures constitute the paradigmatic case, for which the flow stress limit reaches up to $G/20$. A quantitative explanation of the phenomenon is given here with the help of a geometrical model of microstructural development.

**Keywords: work hardening; texture; curling; strain gradient plasticity; BCC and HCP wires; large strains**

## 1. Introduction

Large-strain plastic deformation of polycrystalline matter at low homologous temperature and moderate strain rate, $\varepsilon > 1$, $T/T_{\mathrm{M}} < 0.3$, $10^2\ \mathrm{s}^{-1} > \dot{\varepsilon} > 10^{-5}\ \mathrm{s}^{-1}$, implies strong crystallographic texturing, drastic microstructural refining, dislocation substructuring with concurrent severe work hardening, and building of internal stresses at several scales, together with some degree of macroscopic redundant straining and structural damage (Gil Sevillano *et al*. 1980; Aernoudt *et al*. 1993).

The complexities of the intragranular deformation mechanisms and ensuing three-dimensional dislocation patterns have been highlighted many times, but still look very far from being mastered. Let us call such intragranular plasticity aspects *microscopic*, and let us assume that what happens inside a deforming single-crystal volume element can be abstracted or homogenized when dealing with *mesoscopic size* plasticity problems: by mesoscopic we mean a size or scale covering the compatible deformation of several contiguous grains. Such single-crystalline elements must be small relative to grain size but large relative to characteristic lengths of dislocation substructures, e.g. 10–20 $\mu\mathrm{m}^3$. The mesoscopic scale is assumed to be not so large as

to be able to ignore the influence of deformation compatibility of neighbouring grains on the individual behaviour of the grains. Thus, the possible development and effect of intergranular and intragranular strain differences are to be taken into account. This is, of course, the realm of finite-element method (FEM) type numerical calculations coupled to crystallographic plasticity; however, the present computing capabilities still preclude simulations of the large-strain behaviour of three-dimensional aggregates of differently oriented grains truly representative of real textures (Becker & Panchanadeeswaran 1995; Bate, this issue). In the meantime, some opportunities are left for assessing these problems with more approximate methods. It must also be pointed out that the importance of strain gradients at such dimensional scale levels will make the use of gradient-dependent versions of the plasticity theory unavoidable (Fleck *et al*. 1994; Fleck & Hutchinson 1997) if FEM results are to be meaningful.

In the mesoscopic context, the lowest level of complication occurs when a single-phase, single-crystalline or coarse-grain polycrystalline material is deformed through a strain path that leads to a single-component or to some specially compensated multi-component texture, by means of a process imparting only mild macroscopic redundant strains, which could be minimized through control of the deformation-zone geometry. We can then expect to merely find weak plastic heterogeneities from grain to grain (deviations from the ideal Taylor isostrain approximation, attributable to orientational strengthening, i.e. to differences of their orientation factor, $M(\varepsilon)$), and weak local strain gradients affecting the neighbourhood of grain boundaries arising from more local interactions (both heterogeneities contributing to the Hall–Petch effect prominent at small strain levels). In that situation, which appears to be the most common one, continued strain through stages III and IV leads, asymptotically, towards an absolute strengthening limit below $G/50$ in terms of tensile equivalent flow strength ($M\tau_{\mathrm{s}}^{\mathrm{IV}}$, with $\tau_{\mathrm{s}}^{\mathrm{IV}}$ the saturation resolved critical stress at very large strains, and $M$ an orientation factor close to 3; see Gil Sevillano (1993)). This seems to be the case when rolling high-stacking fault energy face- or body-centred-cubic (FCC or BCC) metals, or when drawing or extruding FCC metals. Processes involving macroscopic redundant strains implying mere simple shear gradients—like ECAE pressing (equal channel angular extrusion) or drawing (Segal 1995; Humphreys, this issue)—or the activation of microscopic heterogeneities in the form of intense simple shear bands in other processes will accelerate the reaching of the saturation stress, but they are not expected to have much more additional strengthening effects, judging by the work-hardening behaviour displayed by such materials in torsion tests (Gil Sevillano *et al*. 1980).

However, even remaining in the single-phase polycrystalline realm, some simple deformation textures are known to promote a strong enhancement of microstructure refinement, coupled to the development of mesoscopic strain gradients of monotonically increasing intensity, the ⟨110⟩ BCC or [0001] hexagonal close-packed (HCP) drawing textures constituting the paradigmatic case. Moreover, such behaviour is accompanied by a sustained work-hardening rate, leading to a remarkable extension of the strengthening limit up to $G/20$ (Langford & Cohen 1969, 1975; Biswas *et al*. 1973; Langford *et al*. 1971).

The extra work hardening comes from a well-known texture-induced difference between the mesoscopic (grain-size range) and macroscopic (sample range) strains (Hosford 1964, 1993). The mutual accommodation of the shape change of neighbouring grains, which must cooperate in building the macroscopic strain, produces typical

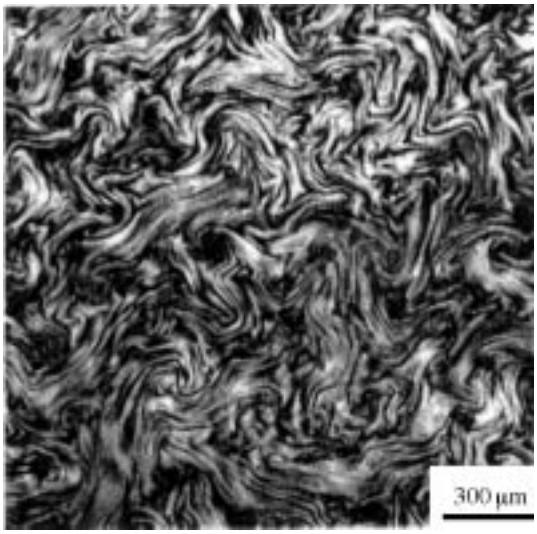


Figure 1. Cross-section of axisymmetrically extruded titanium aluminide (B2 ordered cubic structure), $\varepsilon = 2.77$. The original grain structure was equiaxed (from Thomas *et al*. 1996, with permission from the Institute of Materials).

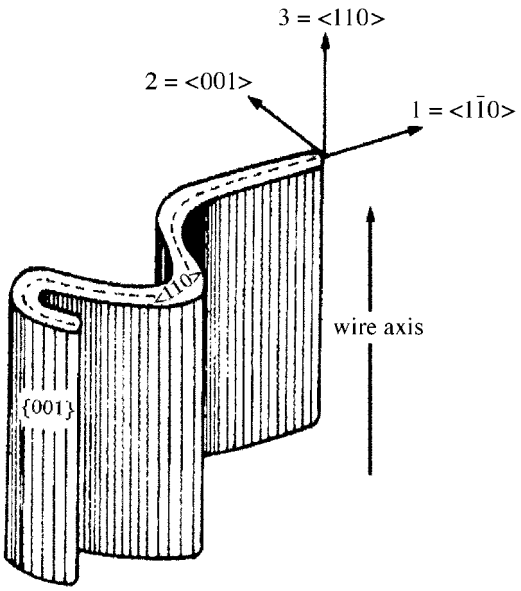


Figure 2. Sketch of the shape adopted by the sections of individual grains in BCC wires with a well-developed ⟨110⟩ fibre texture. The total grain is a very long ribbon, its extended width is of the order of the initial (equiaxed) grain size. Adapted from Hosford (1993).

mesoscopic non-trivial curled grain patterns (also recently christened as VGS, 'Van Gogh sky' structures!; see, for example, Naka *et al*. (1995), Thomas *et al*. (1996) and Gil Sevillano *et al*. (1998), and figures 1 and 2). They require the necessary storage of a grain-size-dependent density of dislocations of the same sign in bent regions of mesoscopic size, much larger than the self-annihilation distance for edge

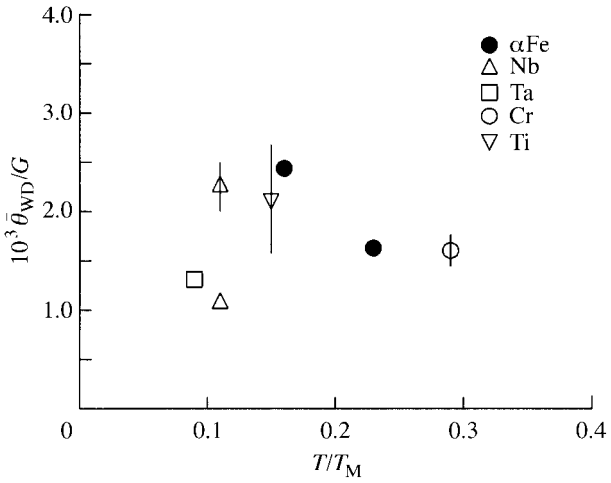


Figure 3. Shear modulus compensated work-hardening rate of several BCC and HCP polycrystalline materials largely strained by axisymmetric elongation by wire drawing versus homologous deformation temperature (Gil Sevillano 1991).

dislocation pairs of opposite sign (Ashby 1970, 1971). Consequently, the strength fraction from such origins is immune to recovery below $0.3T_M$, and the storage of necessary dislocations is determined by a geometrical condition of self-organization of a grain structure, the modulus-compensated work-hardening rate is nearly independent of the base metal being BCC or HCP, its alloy composition or the deformation temperature (figure 3, and see Gil Sevillano (1991) for references).

All these phenomena are discussed in this paper with the help of a geometrical model involving the shape change of a big number of grains. Patterns representative of the grain distortion derived from axisymmetric deformation processes imparted to BCC or HCP polycrystals are simulated from which the extra work hardening is derived. The model is a sort of quasi-continuous upper-bound treatment of the deformation of the polycrystal. The abnormal 'universal' high work-hardening rate associated with curly microstructures is quantitatively explained. Some other interesting information pertinent for performing more accurate (e.g. FEM) calculations of this polycrystalline plastic phenomenon in the future is gathered, e.g. an indication of the minimum number of grains in a section for the results to be truly representative. The presence and consequences of development of local mesoscopic self-organized curly microstructures in other deformation modes, particularly in rolling, are natural further developments of the present work.

## 2. The origin of the curly microstructures in wire-drawn sections of BCC and HCP polycrystals

The origin of grain curling around the elongation axis in axisymmetrically drawn BCC or HCP wires (as well as around the compression axis in axisymmetrically compressed FCC samples) was explained a long time ago. Hosford (1993) recently reviewed the experimental findings and the theoretical reasons that allow us to understand this and other related phenomena (surface effects, i.e. orange-peel, size effect on strength; and roping in ferritic stainless steels). In essence, when microscopic

scale plasticity reasonably obeys the so-called Schmid law, the maximum plastic work principle and its corollaries hold at larger scales. Then the polycrystal finds the mesoscopic strain-rate field resolving the macroscopic strain-rate tensor (with its boundary conditions) with the minimum expenditure of plastic power per unit volume and, of course, only very rarely will the mesoscopic strain-rate field be uniform and coincide with the macroscopic one. A uniform mesoscopic strain-rate field (the Taylor approximation for polycrystal deformation) gives an upper bound for the macroscopic plastic work dissipation rate, or, for the macroscopic stresses or loads, uniform mesoscopic direction in deviatoric stress space (the Sachs approximation) provides a lower bound. When the two bounds for the polycrystal are very different, there is plenty of room for the mesoscopic strain field to strongly deviate from the isostrain-rate condition: intragranular and intergranular strain heterogeneities will develop, at least at that instant of the deformation process. Finite mesoscopic strain heterogeneities will only develop if such a difference persists all along the macroscopic strain path applied to the polycrystalline volume element. *Two conditions are necessary for the continuous growth of finite strain heterogeneities, as follows.*

(a) *The texture* possessing an ample gap between the plastic power dissipation for the mesoscopic uniform-strain hypothesis (the full-constraints condition (FC), in the deformation texture terminology (van Houtte 1984)) and for the uniform stress direction hypothesis (the fully relaxed constraints (FRC) or Sachs condition) *must be stable* along the actual strain path minimizing the plastic work, i.e. the mesoscopically heterogeneous strain path actually chosen by the macroscopic polycrystalline volume. Otherwise, the heterogeneous strain-rate field will continuously change, with lower probabilities of accumulation of finite strain differences from point to point.

(b) *The accommodation strains must have some component* implying mesoscopic shape changes that are *amplified or at least not counteracted by the macroscopic shape change*, because the accommodations, at infinitesimal strain scale, can be viewed as local corrections superimposed on uniform-strain field. This can be easily seen by considering, for instance, that bending accommodations of an elongating axis are weakened by the long-term elongation; by contrast, bending accommodations of contracting directions are amplified.

The case of axisymmetrically drawn BCC (or HCP) wires is a paradigmatic one with respect to these two conditions. The macroscopic strain induces a single-component stable ⟨110⟩ fibre texture from moderate strains (an [0001] in Ti HCP wires), which becomes very sharp after large strains. Individual orientations composing the measured texture are randomly misoriented around the wire axis and the ⟨110⟩ is weakly deviated from this axis (some cyclicity of the texture can be found, particularly at the wire surfaces, with its intensity depending on the deformation-zone geometry employed in the drawing passes). For the BCC ⟨110⟩ or nearby orientations, the ratio of the plastic work for axisymmetric strain versus FRC (Sachs) elongation is very high. If all the critical stresses of the $\{110\}\langle 111\rangle$ and $\{112\}\langle 111\rangle$ slip systems are assumed to have equal value, the ratio of the plastic work equals the ratio of the orientation factors, $M_{\mathrm{FC}}/M_{\mathrm{FRC}}$. This ratio is 1.5 for the exact ⟨110⟩ fibre that is located in a region of the orientation space less than 10° from the orientation maximizing such a ratio ($(M_{\mathrm{FC}}/M_{\mathrm{FRC}})_{\max} = 1.65$). For a texture with a moderate

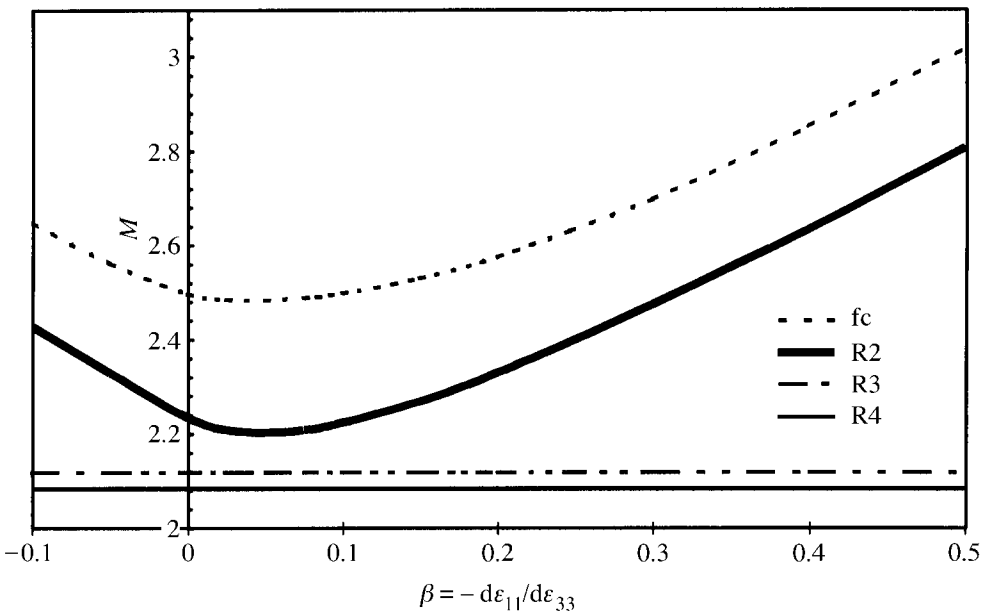


Figure 4. Orientation factors for elongation of a Gaussian texture centred on $[\bar{1}10](110)$ with a standard deviation $s = 16.5°$ in Euler space. The texture can be viewed here as representative either of the orientations of the polycrystal or of a single grain with a misoriented substructure. Meaning of symbols: fc, full-constrained elongation, no shear relaxations; R2, free relaxation of $d\varepsilon_{12}$ and $d\varepsilon_{23}$ shears (parallel to the ribbon surface); R3, free relaxation of $d\varepsilon_{12}$ and $d\varepsilon_{23}$ shears and $(d\varepsilon_{11}/d\varepsilon_{22})$ ratio for each individual orientation; R4, fully relaxed axial elongation (i.e. Sachs).

dispersion around a density maximum in $\langle 110\rangle$, and assuming more realistic relaxed conditions for the individual strains of the grains, owing to the elongated grain morphology, the ratio is still important: of the order of 1.3 (figure 4). By contrast, for the two components of the FCC wire textures, fibres near $\langle 111\rangle$ and $\langle 001\rangle$, the ratio is less than 1.2 and 1.0 for the exact ideal orientations, i.e. sharpening of the texture reduces still further the possibility of cumulative mesoscopic strain heterogeneities.

As for the second necessary condition, inspection of figure 4 shows that the minimum plastic work for any orientation of the approximate $\langle 110\rangle$ fibre occurs for strains close to plane-strain elongation along the axial near the $\langle 110\rangle$ direction and equivalent contraction of the transverse near the $\langle 001\rangle$ direction, the length in the near $\langle 110\rangle$ transverse direction remaining invariant, i.e. for a value $\beta = 0$ of the ratio,

$$\beta = -\frac{d\varepsilon_{11}}{d\varepsilon_{33}}, \tag{2.1}$$

taking the reference system depicted in figure 2, where direction 3 is the axis of the wire. A mesoscopic strain field involving bending implies that different microscopic volume elements of the same grain will be deforming by elongations with a range $(\beta_{\max} - \beta_{\min})$ centred not far from $\beta = 0$ at the neutral axis, with relative freedom for $d\varepsilon_{12}$ and $d\varepsilon_{23}$ relaxations. The range of $\beta$ is limited by the condition that the macroscopic volume average of orientation factor with bending should not surpass the average orientation factor for the texture deforming without bending (i.e. the FC

factor for axisymmetrical uniform deformation, or, better, the corresponding factor allowing for some shear relaxations, R2). We will show that the amount of bending needed for a compatible deformation of an ensemble of grains with ⟨110⟩ texture deforming approximately by plane strain ($\beta = 0$) leads to an orientation factor well below such a theoretical limit (as borne out by the observations!).

## 3. The effect of curly microstructures on work hardening

Mesoscopic plastic strain heterogeneities imply local lattice curvatures, whose sign does not change along regions of extension related to the current grain size. Such curvatures must be resolved by the storage of a density of geometrically necessary dislocations, which, in each microvolume, amounts to a value inversely proportional to an effective local curvature radius, $r_\kappa$,

$$\rho_{\mathrm{curl}} = \frac{M^*}{b_{\mathrm{curl}} r_\kappa}, \tag{3.1}$$

where $b_{\mathrm{curl}}$ is the effective Burgers vector of the dislocations absorbing the local curvature (in the [0001] HCP case, for instance, they are $\langle c + a \rangle$ dislocations on pyramidal systems, the dislocations involved in the pure elongation being $\langle a \rangle$ dislocations on prismatic systems). $M^*$ is an orientation factor relating the curl strain with the crystallographic slip strain in the systems of the geometrically necessary dislocations; it will be larger than unity and its order of magnitude will be 2. In the BCC wires, the curvature is approximately a pure tilt around the wire axis and $r_\kappa$ is the local bending radius as a first approximation (Nabarro 1967).

The curvature radius $r_\kappa$ is related to the current grain size. In general, the relation will be a simple proportionality with the current grain dimension in the direction of the local curvature radius, a function of the strain history times the initial average grain size, $l_0$. Thus, equation (3.1) implies that the extra work hardening arising from mesoscopic heterogeneities will be grain-size dependent, the dependence being, in principle, of the Hall–Petch type.

Now, for $\rho_{\mathrm{curl}}$ to be important, and to remain important, we need to comply with a supplementary condition besides the other two pointed out in the previous section: *initial grain size (or interphase distances in two-phase materials) must be small, and the directions of the curvature radius should not be extended by the macroscopic imposed strain.* The effect will be at a maximum when the direction of the curvature radius is contracted by the macroscopic strain, as is the case in the BCC and HCP wires and related cases. By contrast, in the case of axisymmetric compression of FCC polycrystals, the two conditions for curling manifestation (§ 2) are met, and, indeed, curling of the grains is observed in transverse sections (Hosford 1993). However, the direction of the local curvature radii lies on the plane transverse to the compression axis and the magnitudes of the radii are continuously magnified all along the deformation path, the associated work-hardening enhancement being progressively weakened as strain proceeds. In agreement with this explanation, compressive stress–strain curves of FCC polycrystals do not specially differ from the stress–strain curves obtained along other strain paths where no grain curling is observed (Gil Sevillano *et al*. 1980; Hecker & Stout 1983; Gil Sevillano 1991).

## 4. Calculation of the work hardening of BCC polycrystalline materials at large strains imparted by wire drawing or other axisymmetric elongation methods

### (a) A morphological model of the curly microstructure

If we make a geometrical model of a transverse section representative of a polycrystalline wire deforming by equibiaxial contraction, where each grain has a flexible direction of strain invariant length of initial random orientation, and we map the successive morphologies of the section as their area contracts in the same proportion that their axial dimension elongates, we can extract from its morphological changes all the data needed for calculating an approximation to its macroscopic stress–strain behaviour. If grain contiguity is maintained and grain boundary sliding is forbidden, the value of $\beta$ (equation (2.1)) for each microvolume can be measured, and the average orientation factor for the wire, $M$, calculated using a Taylor FC or relaxed model as done for figure 4:

$$\beta = \beta(\varepsilon), \qquad M = M(\beta).$$

The orientation factor will be a better upper bound than the uniform-strain Taylor factor. Simultaneously, from the local curvature (equation (3.1)), the instantaneous value of the dislocation density originating from curling (i.e. immune to dynamic recovery without long-range diffusion) can be obtained and added to the statistically stored dislocation density, $\rho_s$, assumed to be known,

$$\rho = \rho(\varepsilon) = \rho_s(\varepsilon) + \rho_{VGS}(\varepsilon). \tag{4.1}$$

The value of the critical resolved shear stress can be estimated through the well-known $\tau_c$–$\rho$ relationship (Gil Sevillano 1993), and, then, the volume average of local strengths gives us the macroscopic strength:

$$\Delta\sigma_{VGS} = \sigma(\varepsilon) - \sigma_0 = \bar{M}(\beta)[0.05Gb\sqrt{\rho}\ln(1/b\sqrt{\rho})]. \tag{4.2}$$

A calculation exactly as described above is not easy to perform; we have made an approximate model that does not strictly maintain either the contiguity or the volume of the individual grains but which complies with the macroscopic boundary conditions with local near-plane-strain elongation of the grains, and maintains the constancy of the volume and the contiguity at mesoscopic range (and, of course, at macroscopic level; see Gil Sevillano *et al.* (1998) and Gil Sevillano & Flaquer-Fuster (1996)). The model can be classified as a particular case of a non-intersecting self-avoiding random walk model (Vicsec 1992) starting simultaneously from multiple nuclei.

The model starts with a random distribution of $n_g$ grain nuclei on a plane surface, $A_0$, from which a plausible equiaxed grain structure of the undeformed wire section could be achieved by, e.g. Voronoi tesselation. From each nucleus, a randomly oriented linear segment, of length $\Delta w_0$, small relative to the internuclear distance, $l_0$, is started. From that moment on, new segments are added to the end of the lines with a non-intersecting self-avoiding growth scheme, the orientation of each new segment being determined by the presence of the segments of the other lines and of its own, assuming as the interaction law a repulsive law quadratic with the intersegment distance. No other condition is imposed for growth, the possible range of angles for the new kink of the line being $-\pi < \Delta\Omega < \pi$. The lines are assumed to be the skeletons

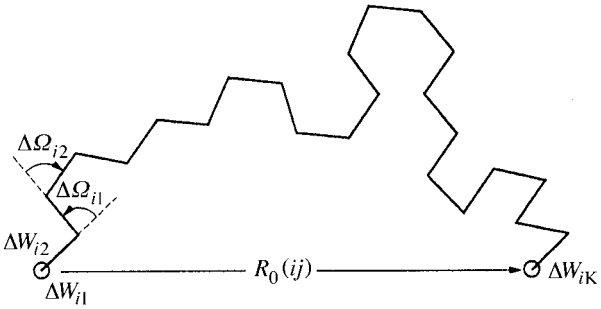


Figure 5. Sketch of the $k$ steps of growth of a grain skeleton line with the definition of its end-to-end distance, $R_0$.

of sections of ⟨110⟩ grains, i.e. the invariant-length directions of the grains that bend around the wire axis. The choice of each new growth direction takes into account an area of influence around the growing segment end containing at least 20 other segments (judged big enough on a trial-and-error basis). The grains are assumed to elongate uniformly in the axial direction and to be initially equiaxed and of the same grain size, $l_0$. Their transverse dimensions, $w$ being the invariant length line and $t$ the thickness, are assumed to vary according to the constancy of the volume:

$$l_0 = (A_0/n_g)^{1/2}, \tag{4.3}$$

$$l_0^3 = lwt, \tag{4.4}$$

$$l = l_0 \exp\varepsilon, \qquad w = l_0. \tag{4.5}$$

In fact, in the numerical calculations, after a very large number of steps, some lines reach an artificial limit for their indefinite growth (again, a compromise between time of calculation and the ratio $l_0/\Delta w_0$ is necessary). On account of this, the true grain dimension along the invariant length direction of each $i$th grain, $w_{ij} \leqslant l_0$, is recorded after each calculation step, $j$, as well as the kink angle formed with the previous segment, $\Delta\Omega_{ij}$ (figure 5). The current grain thickness, $t_{ij}$, is calculated

$$t_{ij} = l_0^2/w_{ij} \exp\varepsilon, \tag{4.6}$$

and the cumulated misorientation absorbed by geometrically necessary dislocations,

$$\Omega_{ij} = \sum |\Delta\Omega_{ij}| = w_{ij}/(r_\kappa)_{ij}. \tag{4.7}$$

From the total misorientation accumulated in the sample after step $i$, $\Omega_i$, the volume (surface, in our case) average curvature, directly linked with the average dislocation density (equation (3.1)), is obtained $(1/r_\kappa)_i$.

The misorientations, in this case of equibiaxial transverse contraction, are scale invariant. The simulated structures have been calculated on the initial sample area $A_0$, so actual linear dimensions on the simulated transverse section must be contracted by a factor $\exp(-\varepsilon/2)$. Consequently,

$$\varepsilon = 2\ln[1 + j(\Delta w_0/l_0)]. \tag{4.8}$$

To minimize edge effects, the area $A_0$ has been taken as the total area of a cube, on which the growing lines can freely walk. The results subsequently presented correspond to simultaneous growth of 1800 lines (grains) with a relative growth segment length per step of $\Delta w_0/l_0 = 1/14$.

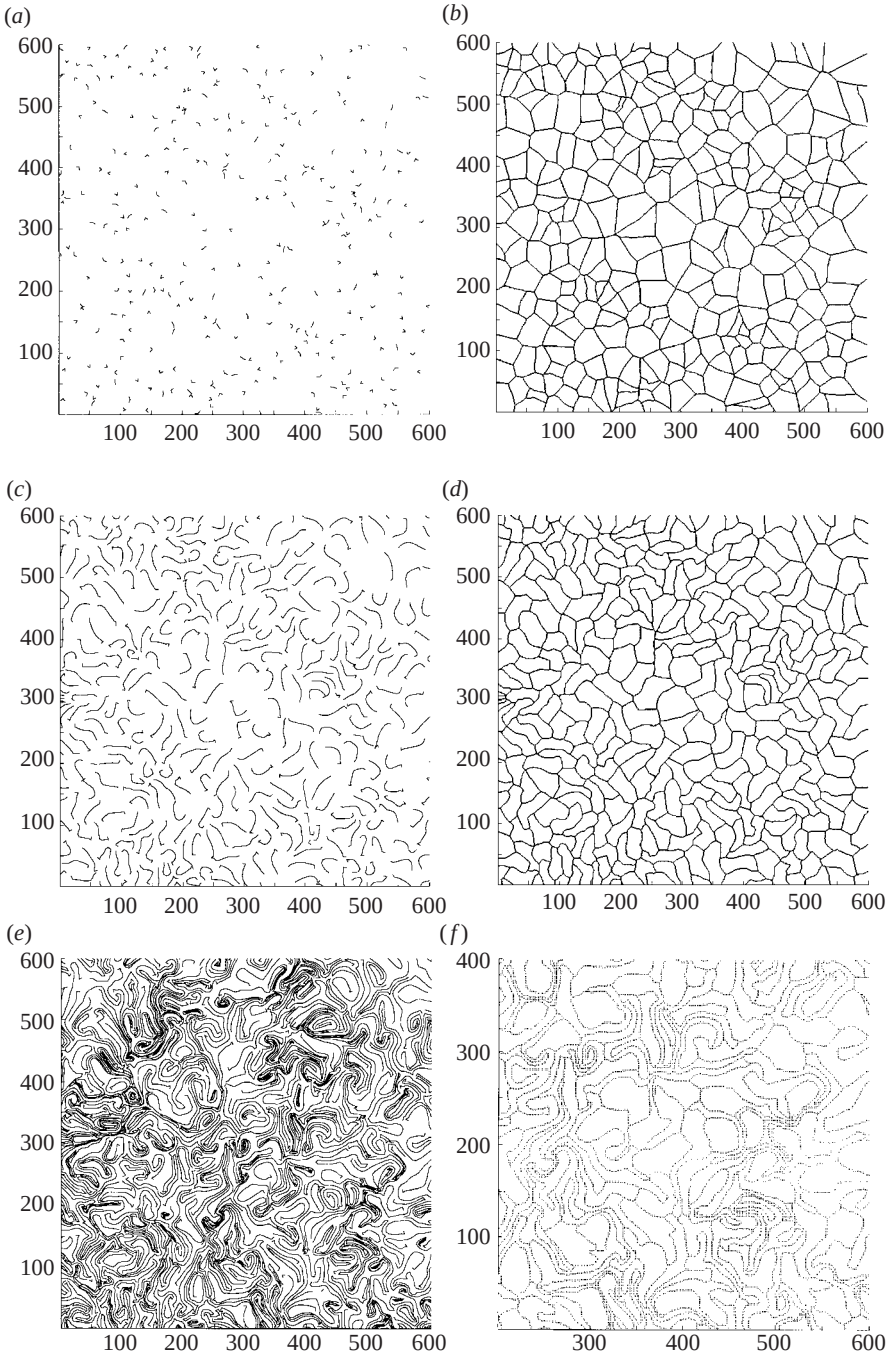


Figure 6. Skeletons corresponding to 300 grains (one face of the cube) for three successive macroscopic strain values, $\varepsilon = 0.27$, 1.08 and 3.05, respectively, together with their corresponding tesselations of the plane (isotropic dilation till impingement). The linear scale is magnified by $\exp(\varepsilon/2)$, the tesselation corresponding to the largest deformation is only a zoom of the lower right of the section.





PHILOSOPHICAL TRANSACTIONS OF THE ROYAL SOCIETY A MATHEMATICAL, PHYSICAL & ENGINEERING SCIENCES

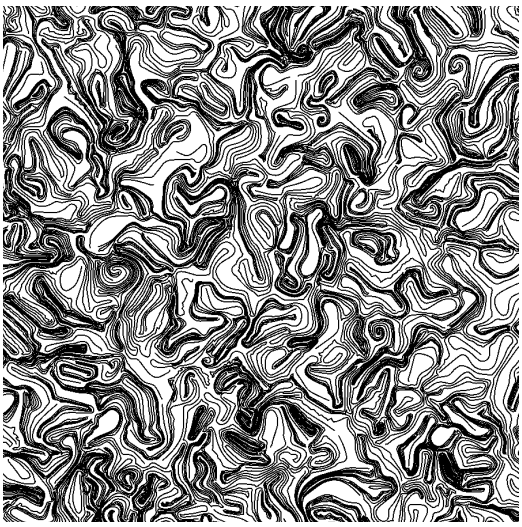

Figure 7. The skeleton lines of another area with 300 grains after a much larger axisymmetric strain, $\varepsilon = 6.4$.

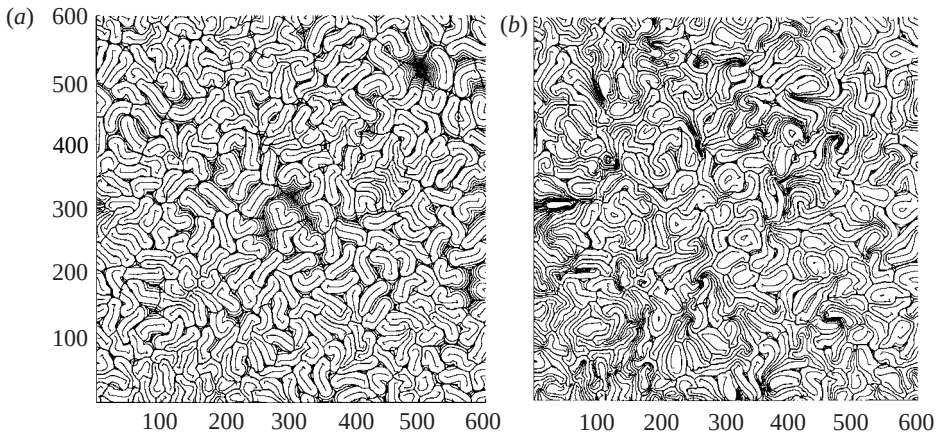


Figure 8. The structures corresponding to $\varepsilon = 1.1$ and 1.8, respectively, where successive dilations from the skeleton (successive fronts at distances in inverse geometric progression) have been shown, together with the final impingement tesselation.

### (*b*) *Results*

Some examples of the microstructures generated are shown in figures 6 and 7. On a qualitative basis, the model mimics, rather well, many observed curly structures, but its limitations are also evident. For instance, the actual grain bending is partly hidden by the tesselations (figure 8), because the model does not completely respect the contiguity of one grain with its neighbours during the simulated deformation process; some grains have bent or even spiralled on themselves.

From the average curvature computed for a sample of 1800 grains, the average dislocation density originated by curling has been computed as a function of strain assuming $M^* = \sqrt{6}$ in equation (3.1) (see figure 9). $M^* = \sqrt{6}$ is the value of the

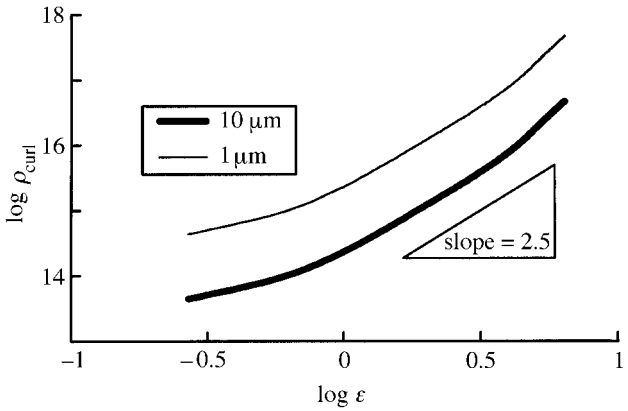


Figure 9. Computed dislocation density originated by curling versus strain, logarithmic scale. The two curves correspond to the indicated starting grain sizes.

orientation factor for plane-strain elongation in the $[\bar{1}10]$ direction (figure 2) and plane-strain bending has been assumed. The value of this factor is only a guess; it depends on the actual configuration adopted by the geometrically necessary dislocations. The Burgers vector $b_{\mathrm{curl}}$ is, here, the $\frac{1}{2}\langle 111\rangle$ lattice dislocation Burgers vector $b = 0.25$ nm (strictly valid for $\alpha$Fe or Cr).

Then, the stress–strain curve has been computed according to equations (4.1) and (4.2) with the same value for the average orientation factor and with a constant value for the statistically stored dislocation density $\rho_{\mathrm{s}} = 10^{15}\ \mathrm{m}^{-1/2}$, of adequate order of magnitude for the saturation of the dislocation density at large strains ($\varepsilon > 1$) in the absence of mesoscopic heterogeneities (Gil Sevillano 1993). The result is presented in figure 10 for two starting grain sizes; for $\varepsilon > 1.5$ the curves are approximately linear (actually an upward curvature is regularly seen in experimental curves when very large strains are reached (see, for example, Langford *et al.* 1971)), and their slopes limit almost exactly the observed range of experimental work-hardening rates of figure 3.

## 5. Discussion

### (*a*) *Validity of the assumptions*

The model mesostructures generated are qualitatively similar to real curly microstructures and, from their geometry, a reasonable prediction of the observed work-hardening rates has been obtained. The conclusion is that the high strengthening capability of wire drawing of BCC metals or HCP Ti alloys is purely related to the particular mesoscopic strain field induced by texture. There is no need for any special microscopic explanation for this behaviour. Previous explanations of this kind, like a kinship with the athermal stage II of single crystals via recourse to the so-called similitude principle (Kuhlmann-Wilsdorf 1970), appear to be redundant. In fact, detailed substructural analysis has shown that here similitude is not obeyed (Langford & Cohen 1975; Langford *et al.* 1971), and the applicability of equation (4.2) is nearly independent of the actual spatial distribution of the dislocation density, be it randomly distributed or forming two-dimensional sub-boundaries (Li 1963). But, for accepting the present explanation, we should check further the validity of the

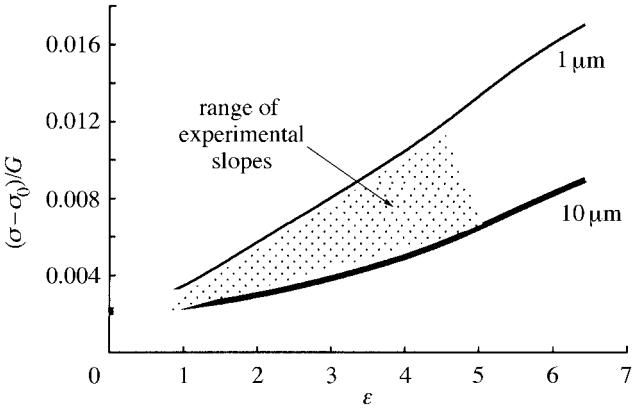


Figure 10. Stress–strain curves for axisymmetrically drawn BCC wires computed for two grain sizes (10 μm and 1 μm) calculated from the geometrical data extracted from simulated curly structures. The assumptions of the model are only valid for large strains ($\varepsilon > 1$), the first part of the hardening, dominated by the statistical storage of dislocations, has not been taken into account. A 'friction stress' term, $\sigma_0$, will be present in experimental curves.

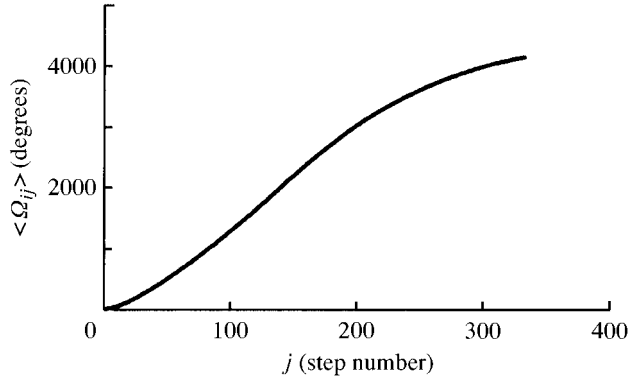


Figure 11. Average accumulated misorientation per chain versus number of growth steps for the simulation reported in this paper.

model. Figure 11 shows the evolution of the mean accumulated misorientation in the sample. The rate of misorientation growth per calculation step increases up to a maximum of $\pi/10$ (18°) for the employed ratio $l_0/\Delta w_0 \approx 14$, for ($j \geqslant 100$, $\varepsilon \geqslant 4$).

Without any assumption about the position of the neutral axis for the bending of the ribbons, from equations (4.6) and (4.7) we have

$$[(\varepsilon_{11})_{\max} - (\varepsilon_{11})_{\min}]_{ij} = (\Delta\varepsilon_{11})_{ij} = t_{ij}\left(\frac{1}{r_\kappa}\right)_{ij} = l_0^2 \frac{\Omega_{ij}}{w_{ij}} \exp\varepsilon \cong \frac{\Omega_{ij}}{\exp\varepsilon}, \tag{5.1}$$

where, as in the rest of the paper, $\varepsilon = \varepsilon_{33}$. On account of equation (4.8), approaching $j$ by a continuum, and averaging for all the grains,

$$(\beta_{\max} - \beta_{\min})_j = \Delta\beta = \frac{1}{4\exp(\varepsilon/2)}\left(\frac{l_0}{\Delta w_0}\right)\left(\frac{d\langle\Omega_{ij}\rangle}{dj}\right) - \frac{\langle\Omega_{ij}\rangle}{(\exp\varepsilon)^2}. \tag{5.2}$$

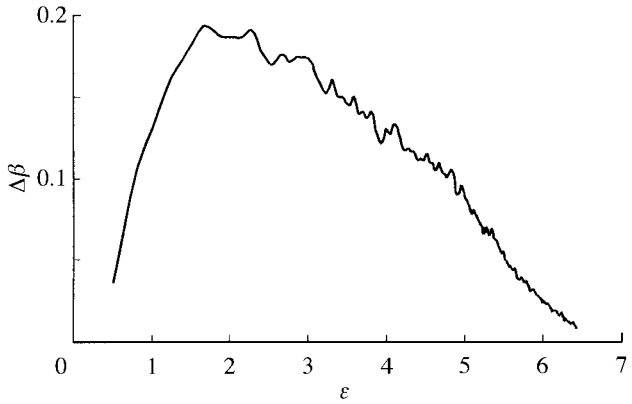


Figure 12. Predicted range of the mean bending strain component of the grains, $\Delta\beta$, as a function of axial strain, $\varepsilon$.

Figure 12 shows the $\beta$ range as a function of axial strain. The location of this range in the abcissae of figure 4 will be such as to minimize

$$\bar{M} = \frac{1}{\Delta\beta}\int_{\beta_{\min}}^{\beta_{\max}} M(\beta)\,\mathrm{d}\beta, \tag{5.3}$$

and the curly microstructure will develop provided $\bar{M} < M$ ($\beta = 0.5$). This is, of course, the case from the beginning of the macroscopic axisymmetric deformation once the $\langle 011\rangle$ texture is well developed in BCC metals. From figure 12 or inspection of equation (5.2), it may also be seen that curling continues to develop at large strains, where the redundant contribution to plastic work steadily decreases and tends to its minimum value.

### (*b*) *Some indications for further improved calculations*

Figure 13 shows the root-mean-squared end-to-end distance of the skeleton lines of the grains (figure 5). It tends to saturate at $R_0 \approx 3l_0$, i.e. for large strains, the region (surface in the cross-section) of interaction of one grain has increased about nine times from its initial value. If a minimum interaction should involve exclusively first neighbours, an absolute minimum for an FEM simulation connecting mesoscopic and macroscopic behaviour should contain, for curly microstructures, at least 60 grains with proper boundary conditions.

The geometry of the simulated curly microstructure provides another more subtle indication about the minimum size required for reproducing the grain interactions leading to this particular mesoscopic behaviour. The curly structure is a case of self-organization, and its geometry shows a fractal behaviour for grain sub-aggregates reaching about three times the average initial intergranular distance. Beyond such range, the geometrical behaviour of the aggregates is trivial (Gil Sevillano *et al.* 1998), i.e. macroscopic. The size $3l_0$ of non-trivial behaviour is coincident with the limit root-mean-squared end-to-end distance of the curly grains referred to above.

### (*c*) *Grain-size dependence of the flow stress and work-hardening rate*

There are few results on the grain-size dependence of the stress–strain behaviour in BCC or HCP wire drawing at very large strains. The results of Biswas *et al.* (1973)

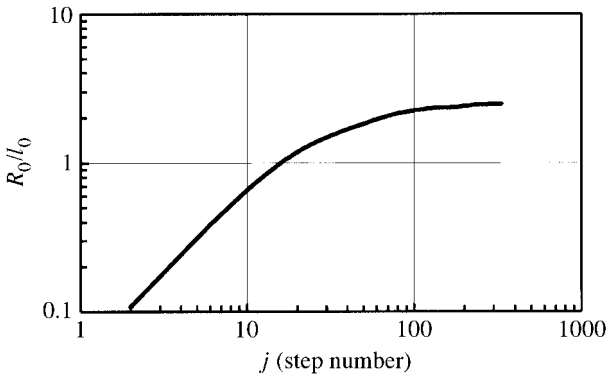


Figure 13. Root-mean-squared end-to-end distance of the skeleton lines of the grains (in units of initial grain size) versus number of calculation steps.

on Ti ($2 < \varepsilon < 4$) do not show any influence of grain size on the work-hardening rate. Those of Morrison & Miller (1970) on low-carbon steel ($2.5\,\mu\text{m} \leqslant l_0 \leqslant 11\,\mu\text{m}$) show an important Hall–Petch-type strengthening between $\varepsilon = 1$ and $\varepsilon = 3$, but the work-hardening rate does not seem to depend on grain size. This is, of course, a question mark for the present model. More experimental results should be gathered covering a large strain range and spanning a wider grain-size range to clarify this point. A possible influence of grain size on texture development should be checked as a tentative explanation for the low sensitivity of the work-hardening rate versus grain size, but this is only a conjecture. The grain subdivision in misoriented blocks at an early deformation stage (Hansen & Juul Jensen, this issue), which is more important for larger initial grain sizes, offers another qualitative explanation for the low grain-size dependence of work hardening observed.

## 6. Conclusions

(1) A geometrical model that approximately reproduces the curly microstructures observed in transverse sections of BCC and some HCP and ordered intermetallics macroscopically deformed by axisymmetric elongation has been developed.

(2) The model is based on the simultaneous growth of self-avoiding non-intersecting walks on a plane surface. The walk lines are taken as the skeletons of the transverse section of grains deforming by near plane-strain elongation and obliged to interfold to maintain mutual compatibility.

(3) From the morphological parameters of the simulated structures, the contribution of the density of geometrically necessary dislocations to work hardening has been computed, giving good agreement with experimental values.

(4) Consequently, the extraordinary retention of an almost athermal quasi-universal high work-hardening rate up to very large strains, discussed here, does not need to be linked to stage II or to any special microstructural processes or principle. Its origin is mesoscopic and probably constitutes an exceptional case.

(5) At first sight, the importance of the contribution of mesoscopic phenomena to macroscopic hardening through other deformation paths (e.g. rolling, shear) in single-phase polycrystals of technical interest does not appear to be so relevant, although some particular ideal textural combinations could show similar effects.

The authors sincerely acknowledge the financial support for this project from the Department of Industry, Agriculture and Fishing of the Basque Government, through project no. 121998. Results of figure 4 were obtained by means of the MTM software for polycrystal deformation, kindly made available by P. Van Houtte, Katholieke Universiteit Leuven (Belgium). The collaboration of T. Gómez-Acebo is also sincerely appreciated. The question of the influence of grain size on work-hardening rate at large strains was raised by B. Hutchinson during the Royal Society meeting.

## References

Aernoudt, E., van Houtte, P. & Leffers, T. 1993 Deformation and textures of metals at large strain. In *Plastic deformation and fracture of materials* (ed. H. Mughrabi), p. 89. *Materials science and technology. A comprehensive treatment* (ed. R. W. Cahn, P. Haasen & E. J. Kramer). Weinheim: VCH.

Ashby, M. F. 1970 The deformation of plastically non-homogeneous materials. *Phil. Mag.* **21**, 399.

Ashby, M. F. 1971 The deformation of plastically non-homogeneous alloys. In *Strengthening methods in crystals* (ed. A. Kelly & R. B. Nicholson), p. 137. London: Applied Science.

Becker, R. & Panchanadeeswaran, S. 1995 Effects of grain interactions on deformation and local texture in polycrystals. *Acta Metall. Mater.* **43**, 2701–2719.

Biswas, C., Cohen, M. & Breedis, J. F. 1973 Strain hardening of titanium by severe plastic deformation. In *Proc. 3rd Int. Conf. on Strength of Metals and Alloys (ICSMA3)*, vol. I, p. 16. London: The Institute of Metals and the Iron and Steel Institute.

Fleck, N. A. & Hutchinson, J. W. 1997 Strain gradient plasticity. *Adv. Appl. Mech.* **33**, 295–361.

Fleck, N. A., Muller, G. M., Ashby, M. F. & Hutchinson, J. W. 1994 Strain gradient plasticity: theory and experiment. *Acta Metall. Mater.* **42**, 475.

Gil Sevillano, J. 1991 Substructure and strengthening of heavily deformed single and two-phase metallic materials. *J. Physique III* **1**, 967.

Gil Sevillano, J. 1993 Flow stress and work hardening. In *Plastic deformation and fracture of materials* (ed. H. Mughrabi), p. 19. *Materials science and technology. A comprehensive treatment* (ed. R. W. Cahn, P. Haasen & E. J. Kramer). Weinheim: VCH.

Gil Sevillano, J. & Flaquer Fuster, J. 1996 Ultra-high strength in-situ composites formed by large strain plastic straining: structure and mechanical properties modelling. *Key Engng Mater.* **127**–**131**, 123. (*Ceramic and metal matrix composites, CMMC'96* (ed. M. Fuentes, J. M. Martinez Esnaola & A. Daniel), part 1. Switzerland: Trans. Tech.)

Gil Sevillano, J., van Houtte, P. & Aernoudt, E. 1980 Large strain work hardening and textures. *Progr. Mater. Sci.* **25**, 69–412.

Gil Sevillano, J., Matey Muñoz, L. & Flaquer Fuster, J. 1998 Ciels de Van Gogh et proprietés mécaniques. *J. Phys. IV France* **8**, Pr 4-155-165.

Hecker, S. A. & Stout, M. G. 1983 Strain hardening of heavily cold-worked metals. In *Deformation processing and structure* (ed. G. Krauss), p. 1. Metals Park, OH: American Society for Metals.

Hosford, W. F. 1964 Microstructural changes during deformation of [011] fiber-textured metals. *Trans. AIME* **230**, 12.

Hosford, W. F. 1993 *The mechanics of crystals and textured polycrystals.* Oxford University Press.





PHILOSOPHICAL TRANSACTIONS OF THE ROYAL SOCIETY A MATHEMATICAL, PHYSICAL & ENGINEERING SCIENCES

Kuhlmann-Wilsdorf, D. 1970 A critical test on theories of work-hardening for the case of drawn iron wire. *Metall. Trans.* **1**, 3173–3179.

Langford, G. & Cohen, M. 1969 Strain hardening of iron by severe plastic deformation. *Trans. ASM* **62**, 623.

Langford, G. & Cohen, M. 1975 Microstructural analysis by HVED of severely drawn iron wires. *Metall. Trans.* A **6**, 901–910.

Langford, G., Nagata, P. K., Sober, R. J. & Leslie, W. C. 1971 Plastic flow in binary substitutional alloys of BCC iron. Effects of wire drawing and alloy content on work hardening and ductiltiy. *Metall. Trans.* **3**, 1843.

Li, J. C. M. 1963 Petch relation and grain boundary sources. *Trans. AIME* **227**, 239–247.

Morrison, W. B. & Miller, R. L. 1970 The ductility of ultra-fine-grain alloys. In *Ultrafine-grain metals* (ed. J. J. Burke & V. Weiss), p. 183. Syracuse, NY: Syracuse University Press.

Nabarro, F. R. N. 1967 *Theory of crystal dislocations*. Oxford University Press.

Naka, S., Marty, M., Thomas, M. & Khan, T. 1995 Variation in the degree of order and its influence on mechanical behaviour in complex B2 aluminides of refractory metals. *Mater. Sci. Engng* A **192/193**, 69.

Segal, V. M. 1995 Materials processing by simple shear. *Mater. Sci. Engng* A **197**, 157–164.

Thomas, M., Naka, S. & Khan, T. 1996 On the very high room-temperature ductility obtained in B2 and/or O-base titanium aluminides. In *Titanium '95: Science and Technology* (ed. P. A. Blenkinsop, W. J. Evans & H. M. Flower), pp. 388–395. London: The Institute of Materials.

van Houtte, P. 1984 Some recent developments in the theories for deformation texture prediction. In *Proc. ICOTOM 7 (7th Int. Conf. on Textures of Materials)* (ed. C. M. Brakman, P. Jongenburger & E. Mittemeijer), p. 7. Noordwijkerhout: The Netherlands Society for Materials Science.

Vicsec, T. 1992 *Fractal growth phenomena*, 2nd edn. Singapore: World Scientific.





PHILOSOPHICAL TRANSACTIONS OF THE ROYAL SOCIETY A MATHEMATICAL, PHYSICAL & ENGINEERING SCIENCES

PHILOSOPHICAL TRANSACTIONS OF THE ROYAL SOCIETY A MATHEMATICAL, PHYSICAL & ENGINEERING SCIENCES